Supplemental figure legends

Supplemental Figure 1 Isolation and characterization of *ex vivo* culture of primary prostate fibroblasts

A) RP tissue wedges (i) containing regions of suspected malignancy and benign-adjacent tissue are sampled (ii) using 4 mm^3 biopsy punchers. The top part of each biopsy core is removed (iii) for FFPE processing (iv) and subsequent histopathological evaluation. Remaining tissue is quartered (v) and similarly processed. B) Histopathological validation of the top section of biopsy cores from (Aiii-iv) via HE staining and p63 (brown) and AMACR (red) dual-immunohistochemistry. C) The remaining biopsy core is cut into small pieces and transferred to culture medium that supports fibroblast but not endothelial cell growth. Outgrowing fibroblasts are selectively enriched away via trypsinization from any epithelial cells, which require additional collagenase treatment for detachment. D) Representative images of three primary fibroblast explant cultures isolated from different patients stained for mesenchymal markers vimentin (green) and CD90 (white) and the epithelial marker pan-cytokeratin (red). Nuclei were counterstained using Hoechst (blue). 22Rv1 PCa cells served as positive control for pan-cytokeratin (*far right, upper panel).* Negative control of a parallel stained fibroblast culture incubated without primary antibodies (*far right, lower panel).*

Supplemental Figure 2 *Ex vivo* culture of primary prostate fibroblasts – pertaining to Supplemental Fig. 1

Single channel monochromatic images (from Supplemental Fig. 1D) of immunofluorescent validation of three primary fibroblast explant cultures isolated from different patients stained for mesenchymal markers vimentin (green) and CD90 (white) and the epithelial marker pan-cytokeratin (pan CK, red). Nuclei were counterstained using Hoechst (blue). 22Rv1 PCa cells served as a positive control (pos. ctrl) for pan-cytokeratin. Negative control (neg. ctrl) of a parallel stained fibroblast culture incubated without primary antibodies (*far right, lower panel).*

Supplemental Figure 3 Transcriptomic analysis of primary prostate fibroblast cultures identifies two distinct CAF populations - pertaining to Figure 1

A) Heatmap depicting sample level expression of significantly upregulated genes (*P.*adj<0.05, log2FC>0.3) for each fibroblast cluster (related to Fig. 1C). B) clusterProfiler analysis of *Left:* GO Biological Process for significantly upregulated genes of each fibroblast cluster, including two cycling CAF explant cultures (cycling) (related to Fig. 1A-B), *center and right*: the top 20 scoring Hallmark and REACTOME pathways for significantly upregulated genes of each fibroblast cluster (related to Fig. 1J-K), respectively. C-D) Expression of the indicated genes across each fibroblast cluster. Values denote C) average log2 signal intensity from quartile normalized bulk transcriptomic data and D) mean $2^{-\Delta Ct}$ via qRT-PCR relative to the housekeeping gene *TBP*. Error bars denote S.E.M. Significance was calculated via a Kruskal-Wallis test with multi-comparison correction using the two-stage linear step-up method of Benjamini, Krieger and Yekutieli. Significance is denoted **, *P*<0.01; ***, *P*<0.001. E) Comparison of expression profiles for each fibroblast cluster with published scRNA-seq datasets using combined z-scores for each gene signature and represented as mean per fibroblast cluster (related to Fig. 1H-I). *Left:* Heatmap with rows clustered by correlation to depict similarities between different gene signatures. *Right:* Dotplot with color representing combined z-scores and dot size inversely proportional to standard deviation (S.D.) to depict variability within each cluster. F) Sample level heatmap showing expression levels of genes annotated to the interferon gamma response Hallmark pathway (related to Fig. 1L). G) Expression of signature genes (combined z-score) for each primary fibroblast cluster in the TCGA prostate adenocarcinoma (PRAD) cohort (related to Fig. 1N-O). Boxplots were used to compare signature gene expression levels across Gleason scores, T and N stages and biochemical recurrence (related to Fig. 1N-O, Q). The R package ggsignif [74] was used to perform t-tests. Source data for panels A-C, E-G are provided in the Source Data file.

Supplemental Figure 4 Identification of multiple fibromuscular cell populations *in situ* - pertaining to Figure 2

A) Relative distribution of fibroblast (F) and mural cell (M) subclusters in re-clustered fibromuscular scRNA-seq [22] per A) patient or B) sample. C) 2D visualization (UMAP dimensionality reduction) of the fibroblast and mural cell subpopulations (related to Fig. 2E). D) Feature plots showing the expression Ucell scores for fibroblast and mural cell gene signatures derived from [23, 66] or the canonical fibroblast and mural cell markers *PDGFRA* and *MCAM*, respectively. E) Dotplot showing average expression for the fifteen most significant (*P.*adj) markers of each mural cell (M) subpopulation. Dot size is inversely proportional to standard deviation (S.D.) to depict variability within each cluster. F) Violin plot depicting expression of selected marker genes demarcating distinct mural cell subclusters. G) Frequency of each mural cell subpopulation relative to the total number of mural cells according to the histopathology status of the corresponding tissue sample wherein the presence or absence of PIN, inflammation and/or cancerous cells was defined as activated *vs.* non-activated tissue, respectively (related to Fig. 2D). H) Violin plot depicting expression of selected marker genes demarcating distinct fibroblast (F) and mural cell (M) subclusters (related to Fig. 2B). I) Dotplot depicting the expression level of published fibroblast and mural cell gene signatures for each fibroblast subpopulation (related to Fig. 2I). Ucell scores calculated for each gene signature are represented as scaled mean per subcluster with dot size inversely proportional to standard deviation (S.D.) to depict variability within each cluster. J) Representative images of negative (*dapB*) and positive *PPIB* (blue) and *POLR2A* (red) control probes for Duplex-ISH images shown in Fig. 2G and 2J. K) Dotplot representing average expression of the canonical peri-epithelial and interstitial human prostate fibroblast genes *APOD* and *C7*, respectively from [16] across all fibroblast subpopulations (related to Fig. 2C). L) Duplex-ISH of human PCa *(right panels)* and benign-adjacent tissue *(left panels)* sections using the RNA probes indicated, whereby font color corresponds to staining color. Sections were counterstained using hematoxylin. Scale bars represent 50 µm *(top panels)* or 25 µm *(middle and lower panels)*. Images are representative of four independent experiments using tissue sections from three different patients. M) Expression of signature genes (combined z-score) for the indicated mural cell (M) subpopulation in the TCGA-PRAD cancer or normal prostate tissue cohorts (related to Fig. 2K). N)

Kaplan-Meier curves generated using GEPIA2 depicting DFS on the TCGA-PRAD cohort using the five most upregulated M5-specific genes and upper/lower quartiles as group cut-off. O) Expression levels (combined z-score) of the most significantly (*P.*adj F3 and F5) upregulated subpopulation-specific genes in the TCGA-PRAD cancer cohort. Boxplots were used to compare Gleason score, T and N stage and biochemical recurrence. M, O) The R package ggsignif [74] was used to perform t-tests. Statistical significance is denoted NS., not significant; *, $P<0.05$; **, $P<0.01$; ***, $P<0.001$. Source data for panels A-B, D-E, G, I, M-O are provided in the Source Data file.

Supplemental Figure 5 Differential expression of PLN, CCDC102B and CNN1 distinguish mural cell subtypes in human prostate cancer and benign-adjacent tissue

A) Feature plots of the indicated mural cell markers. B-E) Multiplex immunofluorescent staining of human PCa tissue sections and patient-matched benign-adjacent areas using the antibodies indicated whereby font color denotes pseudo-coloring in the displayed merged images. Nuclei were counterstained using Hoechst 33342 (blue). B) Upper left: cells positive for the M1-specific marker PLN are double positive for the pan mural cell marker MCAM and surround $CD31^+$ endothelial cells in benign-adjacent tissue whereas $MCAM^+$ parenchymal SMCs lack PLN. Upper right: large but not smaller $CD31^+$ blood vessels (arrowheads) in high-grade PCa also comprise a layer of $PLN^+/MCAM^+$ vascular SMCs. Loss of MCAM immunopositivity in parenchymal but not vascular SMCs in high grade PCa. Lower panels: due to strong differences in expression levels of MCAM between vascular and parenchymal SMCs, enlarged images of orange boxed regions (*upper panels)* were acquired using shorter exposure times for better visualization. C) Left: a single layer of pericytes surrounding smaller $CD31^+$ vessels are demarcated by $MCAM^+/CCDC102B^+$ double immuno-reactivity in high-grade PCa *(left panel)* and benign-adjacent tissues (not shown). Right: enlarged image of the boxed region (*left panel)* is shown (the MCAM signal was omitted for better visualization). Residual parenchymal SMCs are detected as non-vessel associated $CCDC102B^+$ cells, which in some cases retain MCAM co-expression. D) Parenchymal SMCs are positive for the M5/M3 marker CCDC102B as well as CNN1. In

benign-adjacent tissues (*left panels)*, prominent intercellular MCAM immuno-reactivity is observed between SMCs, which display a compact morphology and are arranged into organized, densely packed bundles. In malignant tissues (at the invasive front and in the tumor core), there is a prominent loss of intercellular MCAM immuno-positivity particularly in the peri-epithelial space and dispersal of SMC bundles. Residual parenchymal SMCs exhibit an elongated morphology and are frequently present as single, isolated cells. Lower panels represent enlarged images of boxed regions (*upper panels)*. E) Enlargement of the pink boxed region (upper left panel D, indicated #) showing rounded, strongly positive CCDC102B^{+} cells that are frequently observed within MCAM^{+} lymphatic vessels of benign-adjacent tissues and less commonly in malignant foci. Shorter image acquisition times were used for better visualization, which reveals a nuclear structure highly reminiscent of granulocytes. F) Table summarizing the three main mural cell subtypes present in the benign-adjacent/malignant human prostate and their relative expression of the marker combinations that can be employed to distinguish them (cvSMC, contractile vascular SMC; pSMC, parenchymal SMC). Original magnification 20x (B-D), 63 x (E). Images are representative of at least five independent experiments using tissue sections from five different patients.

Supplemental Figure 6 The transcriptomic profiles of *ex vivo* primary human prostate CAF explant cultures recapitulate distinct human prostate CAF subpopulations *in vivo* - pertaining to Figure 3

A-B) Sample level heatmaps showing expression of scRNA-seq fibroblast (A) or mural cell (B) cluster signature genes (log2FC ranked) genes of each in the bulk transcriptomic explant dataset (related to Fig. 3B). C) Dotplots depicting expression levels of general activation/contractile markers and PCa CAF subpopulation-specific genes in the indicated fibromuscular clusters of the scRNA-seq dataset (related to Fig. 3C). PCa-iCAF denotes CAF1/F3-specific genes, PCa-myCAF denotes CAF2/F5/M5-specific genes. Color denotes average expression and dot size is inversely proportional to the percentage of expressing cells, respectively. D-E) Sample level heatmaps displaying expression of general activation/contractile markers, PCa-iCAF- and PCa-myCAF-specific genes in D) the indicated

fibromuscular clusters of the scRNA-seq dataset (related to Fig. 3C and Supplemental Fig. 6C) or E) the bulk transcriptomic explant culture subpopulations. F) Sample level heatmaps of qRT-PCR-derived $2^{-\Delta CT}$ expression values of the indicated genes in the original 38 samples of the bulk transcriptomic explant dataset (*left)* and an independent cohort of 32 primary human prostate explant cultures *(right)* (related to Fig. 3D). G) Single channel monochromatic images (from Fig. 3E) of immunofluorescent validation using antibodies against PDPN (PCa-iCAF marker), ITGA11 (PCa-myCAF marker) and SMA/ACTA2 in three different primary human prostate explant cultures that clustered in the independently qRT-PCR-validated cohort (depicted in Fig. 3D) into NAF, CAF1 or CAF2 substates. Original magnification 200 x. Images are representative of three independent experiments using explant cultures from seven different patients. H) DFS heatmap generated using GEPIA2 depicting log10 HR for the indicated genes across TCGA cohorts for all available cancer types. Median expression level was used as group cut-off. Statistically significant differences are boxed (related to Fig. 3F). Source data for panels A-F and H are provided in the Source Data file.

Supplemental Figure 7 Functional characterization of *ex vivo* primary CAF substates reveals plasticity and distinct hallmarks yet shared onco-supportive capacities – pertaining to Figure 4

A) Proliferation assay of the indicated PCa cell lines incubated for 96h with CM from primary CAF1 or CAF2 cultures and patient-matched NAFs (related to Fig. 4A). Non-conditioned media (nonCM) incubated for the same duration without primary fibroblasts served as control. Data represent mean fluorescence of quadruplicate wells from six independent experiments using primary explant cultures derived from six different donors. B) qRT-PCR analysis of the indicated genes normalized to the housekeeping gene TBP in CAF2 cells cultured on 2 kPa elastic hydrogels for 72h relative to standard tissue culture plasticware. Data represent mean fold change in gene expression from three independent experiments using cells isolated from 4 different donors. C) Human Protein Atlas [36] (version 23.0; https://www.proteinatlas.org/) immunohistochemistry images from PCa tissues of indicated pathology stained with anti-FN1 (HPA027066), -FBLN1 (CAB004393) or -COL1A1

(HPA011795) antibodies (https://www.proteinatlas.org/ENSG00000115414-FN1/pathology/prostate+cancer#img; https://www.proteinatlas.org/ENSG00000077942-FBLN1/pathology/prostate+cancer#img; https://www.proteinatlas.org/ENSG00000108821-COL1A1/pathology/prostate+cancer#img). A-B) Statistical significance was calculated via: A) one sample two-tailed T test, B) one-way ANOVA using Tukey multiple comparison correction. Significance is indicated *, $P<0.05$; **, $P<0.01$; ***, $P<0.001$.

Supplemental Figure 8 Multiplex immunofluorescent staining of human PCa reveals distinct patterning of CAF subpopulations – pertaining to Figure 5

A-F) Human prostate tissue sections of indicated pathology were stained using the antibodies shown. Font color denotes pseudo-coloring in the displayed merged images. Nuclei were counterstained using Hoechst 33342 (blue). Original magnification 200x. Boxed regions are shown enlarged beneath (A-B) or to the right (C and E) of each parental image. C) Orange triangles denote putative pc-like myCAFs, which display an elongated fibroblast-like morphology and co-expression of the M5-enriched mural cell marker CCDC102B and F5-enriched myCAF marker ENG. E) Boxes marked with a broken or solid line are enlarged in the center and right panels, respectively. For improved visualization, AR brightness was enhanced in the enlarged images (center and right panels) and image overlays display only the indicated markers. F) Negative control incubated without primary antibodies. A-F) Images are representative of 4 independent experiments using tissue sections derived from 8 different patients.

Supplemental Figure 9 Dynamic remodeling of CAF activation states *in vivo* - pertaining to Figure 6

A) Sample level heatmaps depicting expression level of the corresponding murine orthologs for the indicated explant culture/scRNA-seq subcluster signature genes (Fig. 3C) in the mouse transcriptome of castrated and intact samples from the indicated PDX model. *Left,* BM18 only; *center*, LAPC9 only; *right*, BM18 and LAPC9 models. B-C) Single channel monochromatic images of images displayed in Fig. 5D of the indicated PDX tumor using the antibody indicated.

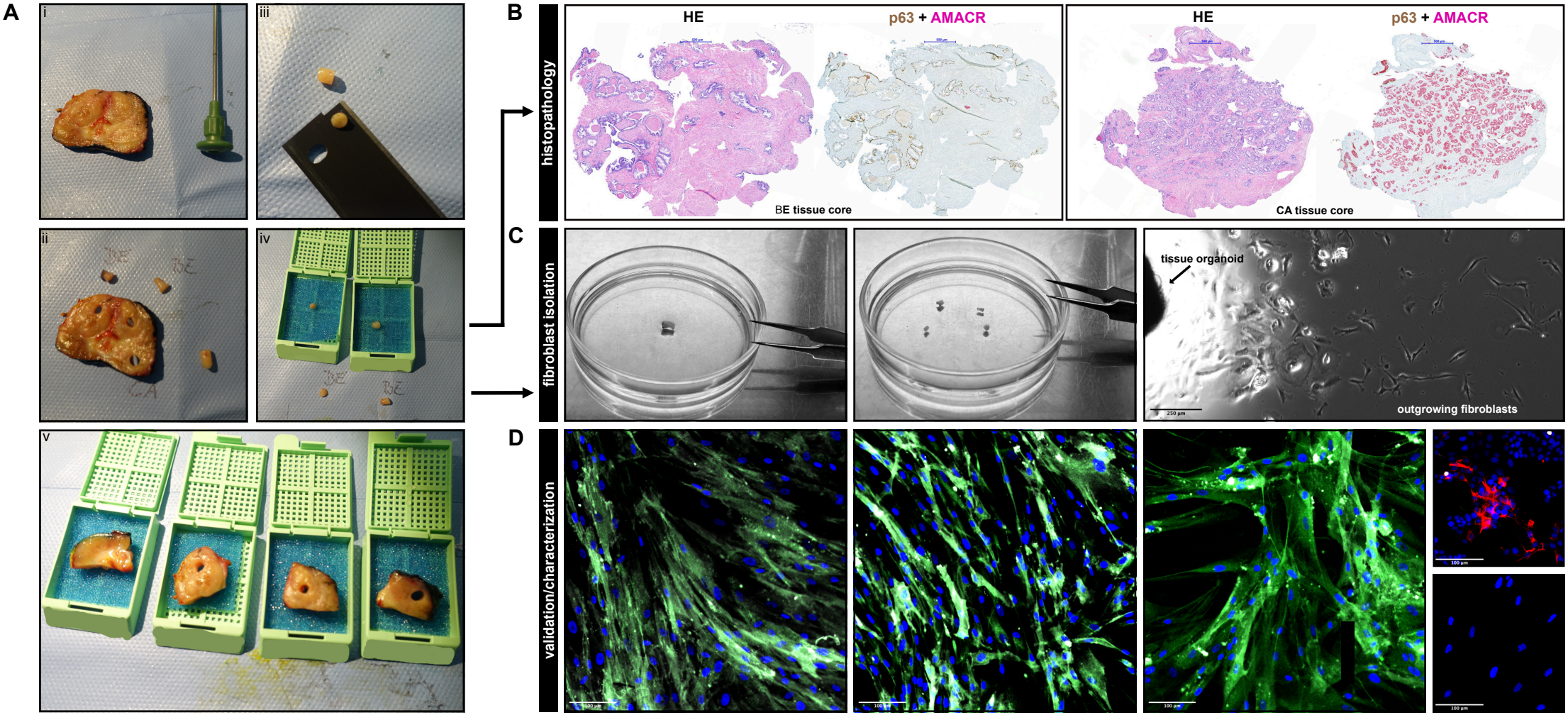

Supplemental Fig. 1

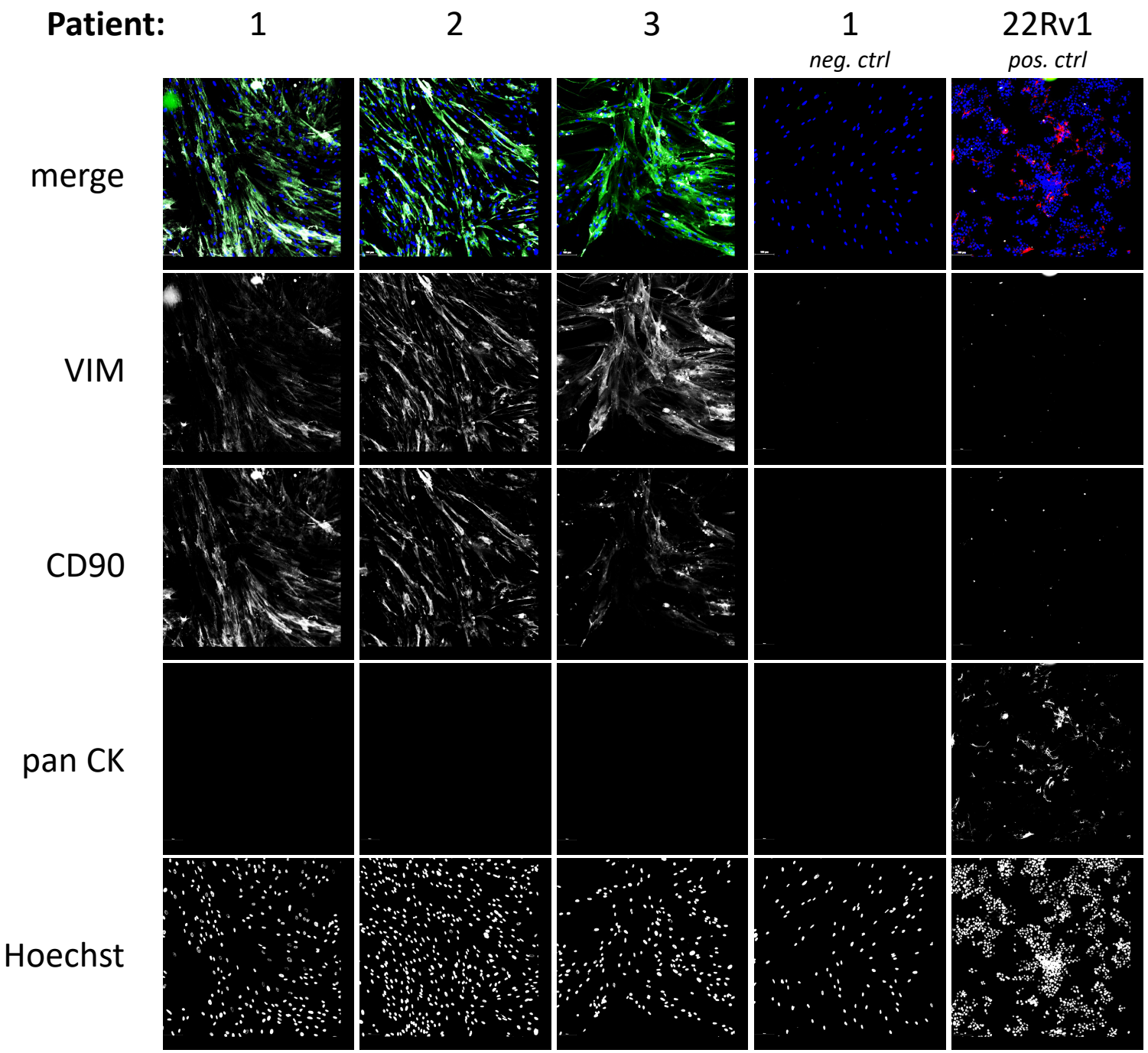

Supplemental Fig. 2

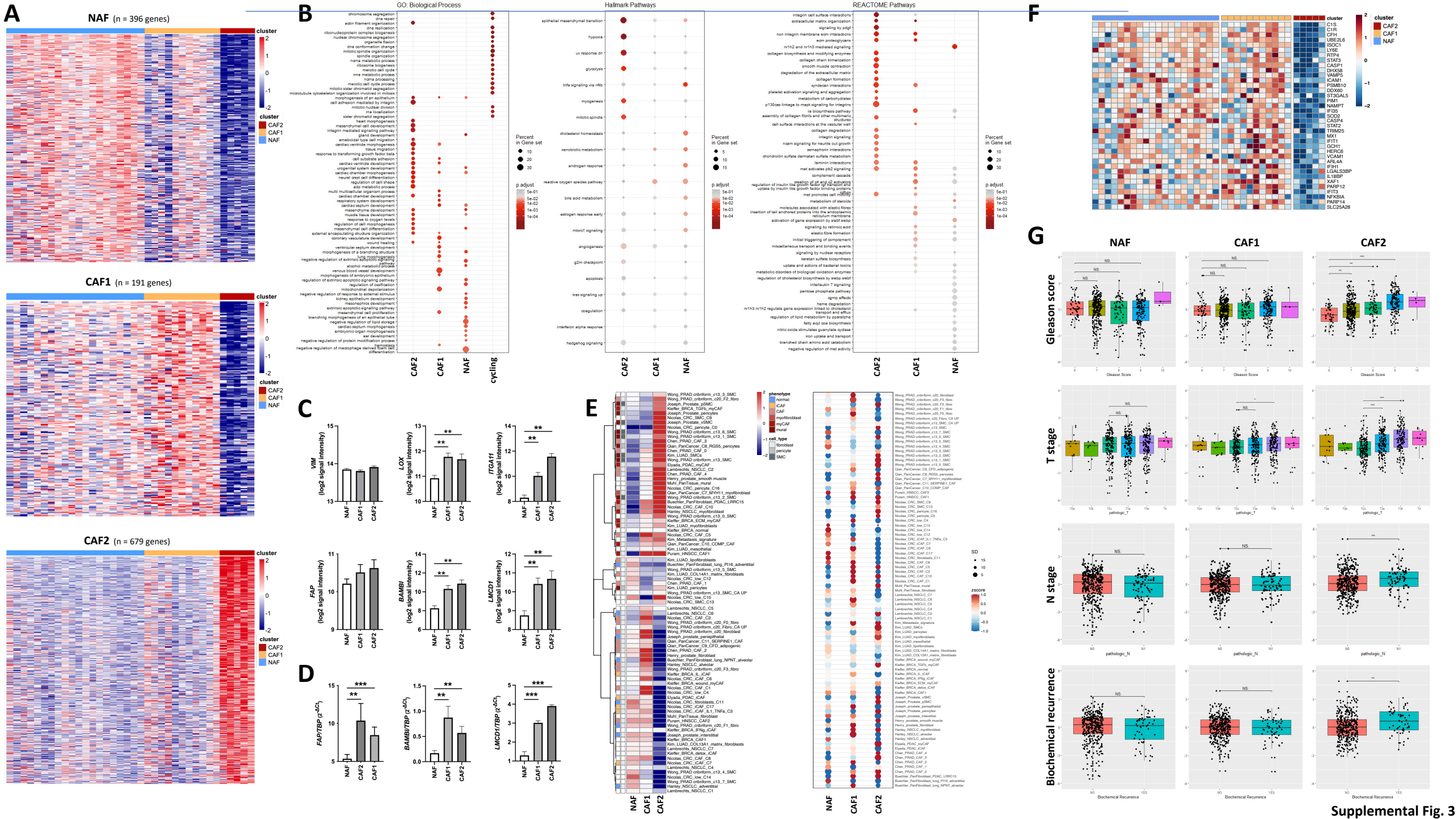

Supplemental Fig. 3

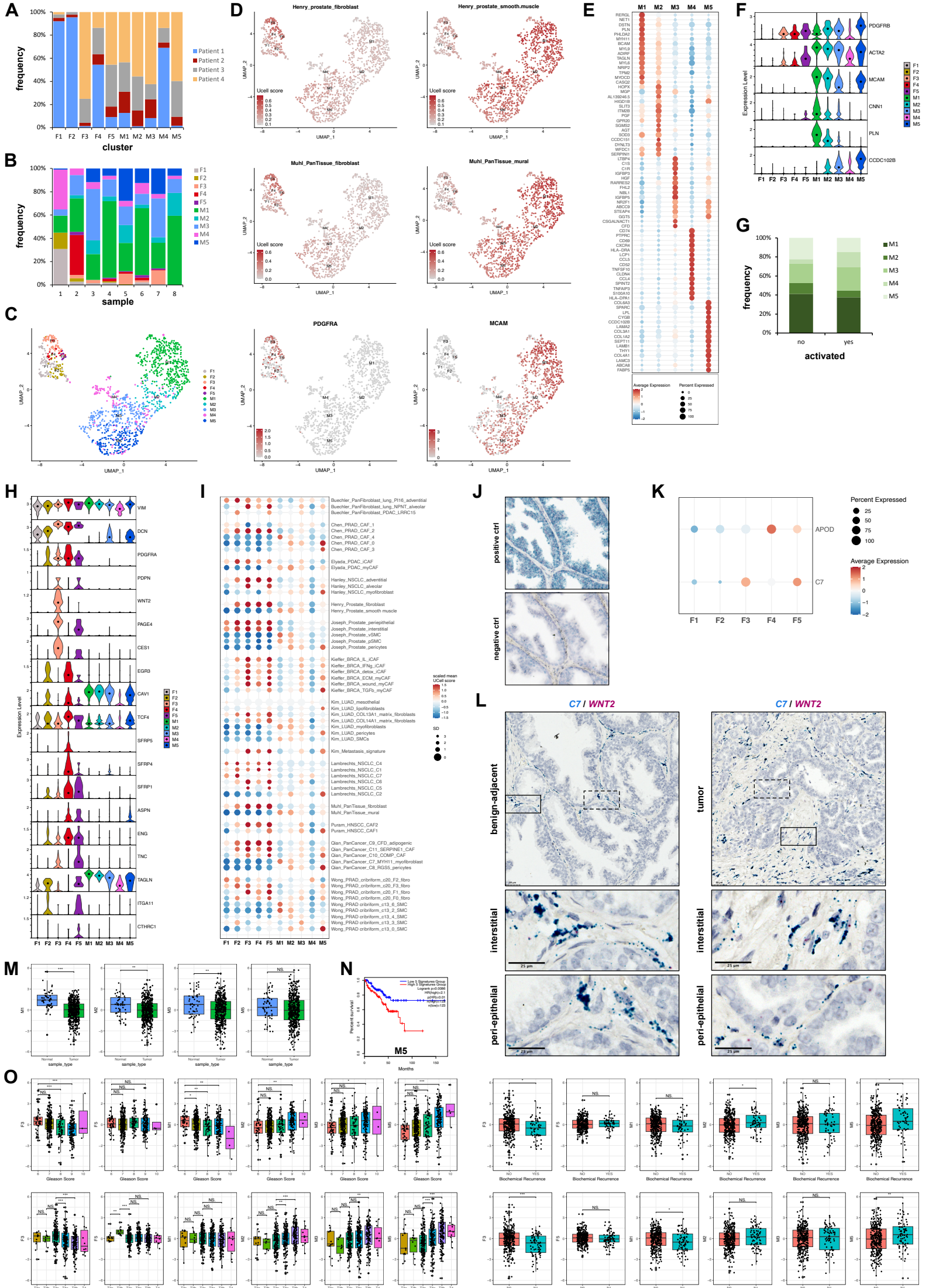

Supplemental Fig. 4

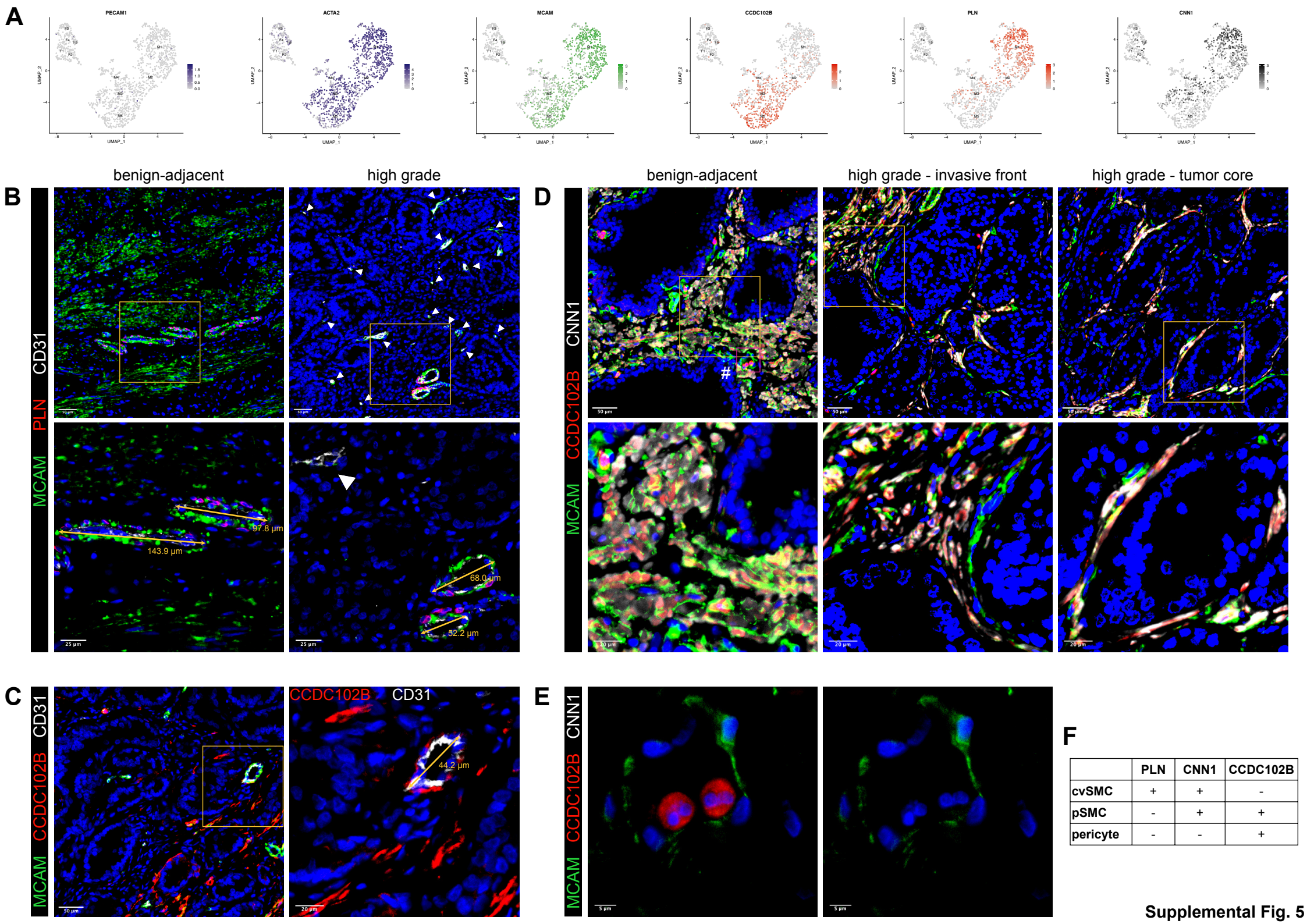

	PLN	CNN1	CCDC102B
cvSMC	+	+	-
pSMC	-	+	+
pericyte	-	-	+

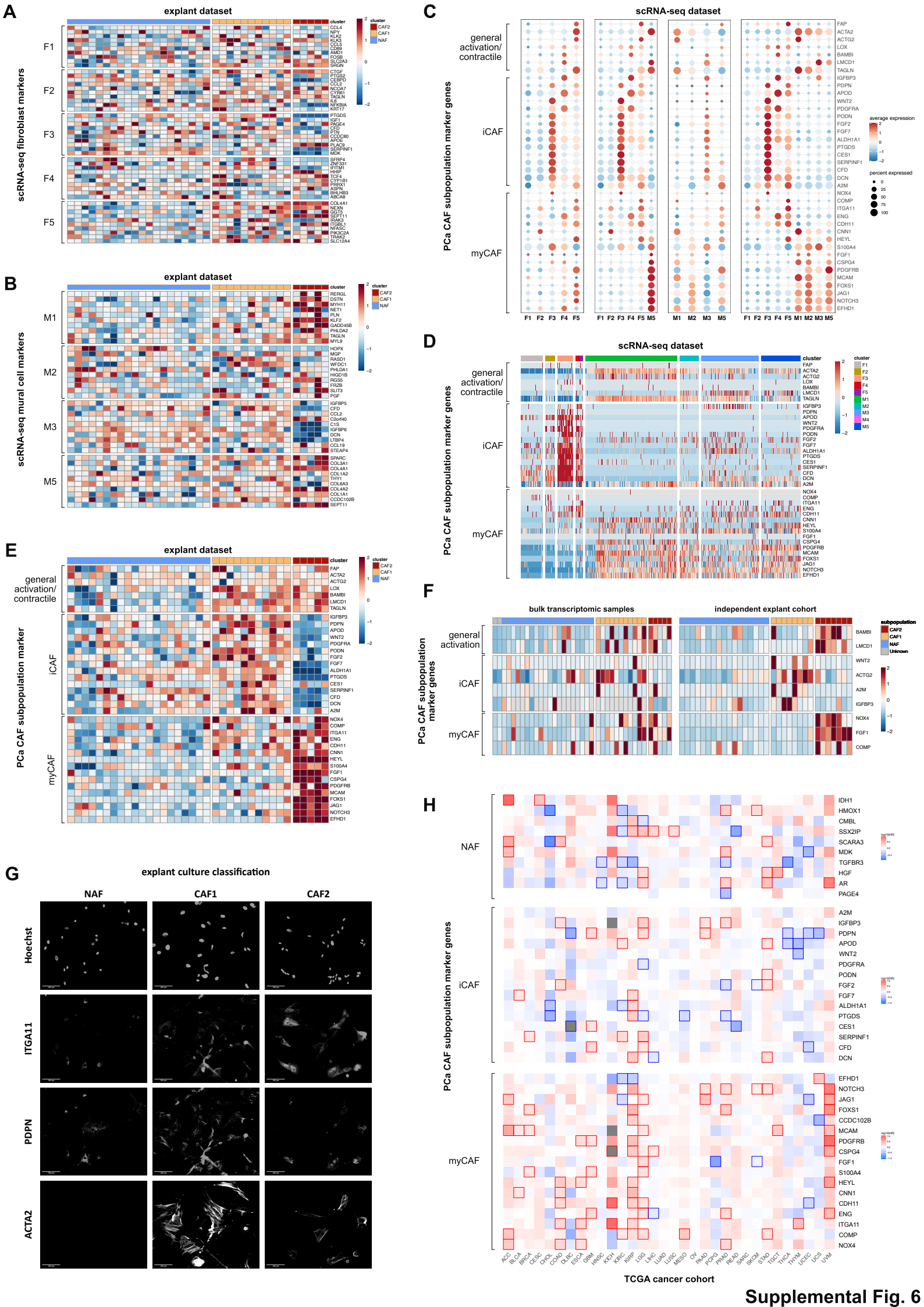

Supplemental Fig. 6

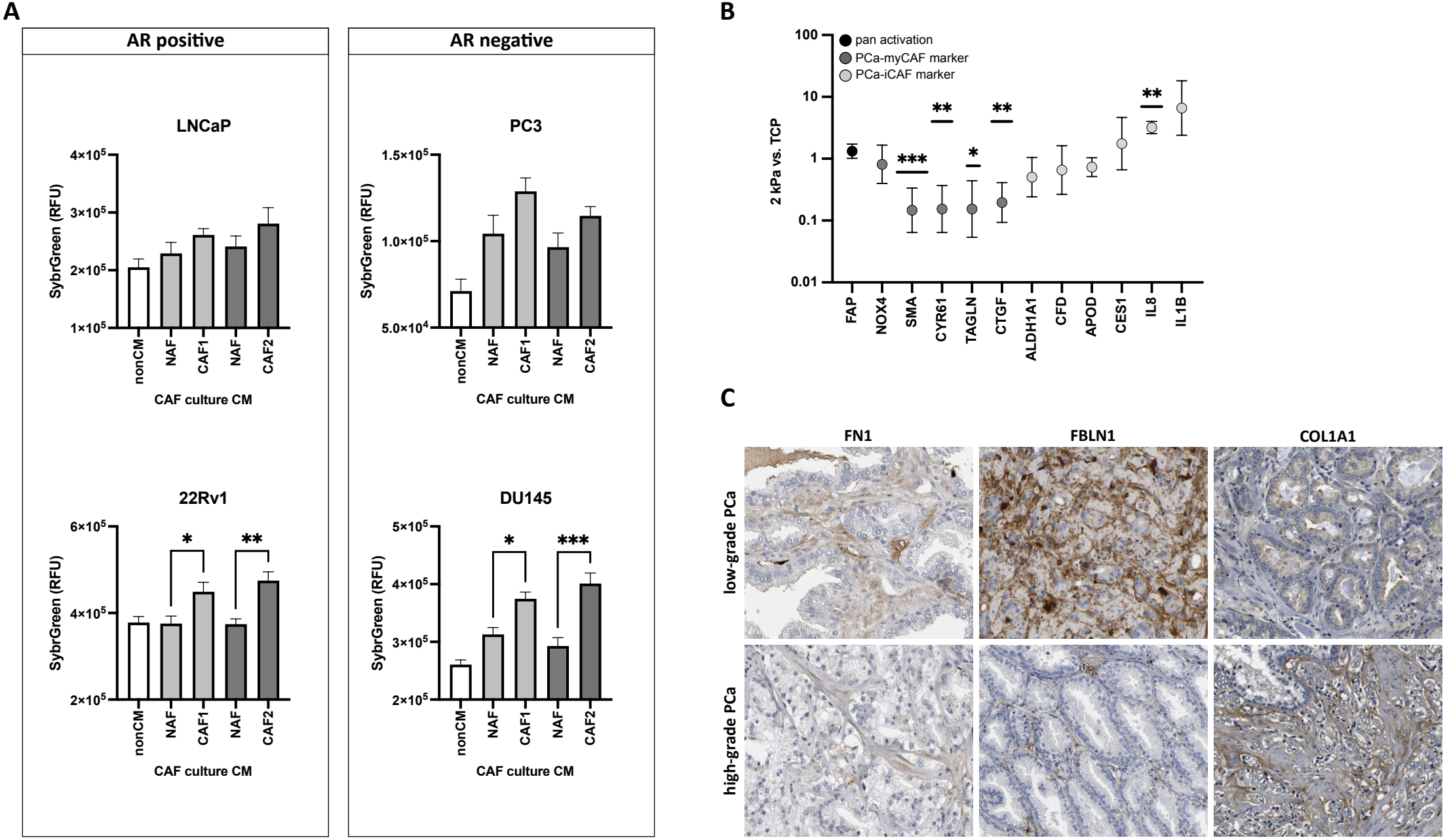

Supplemental Fig. 7

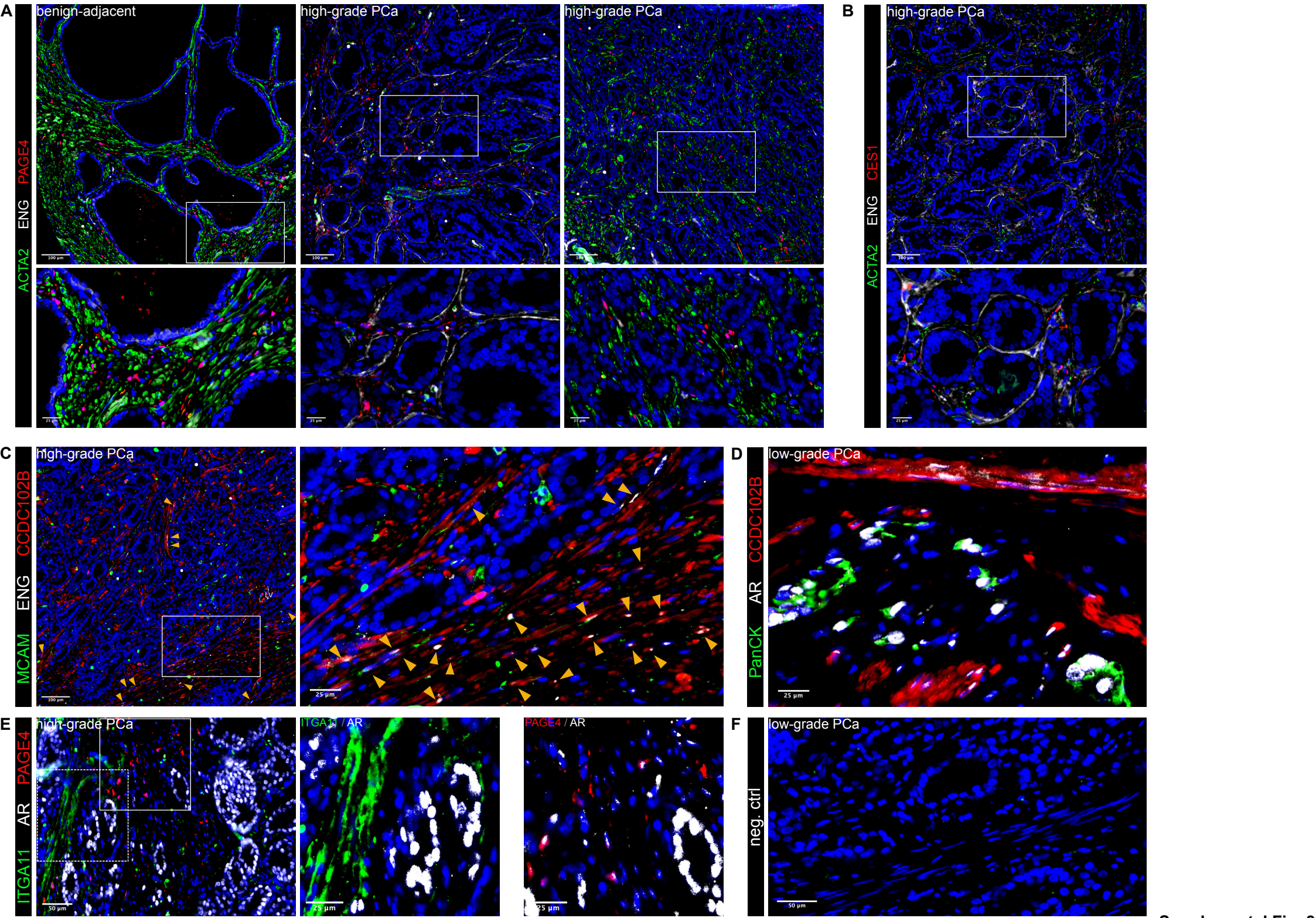

Supplemental Fig. 8

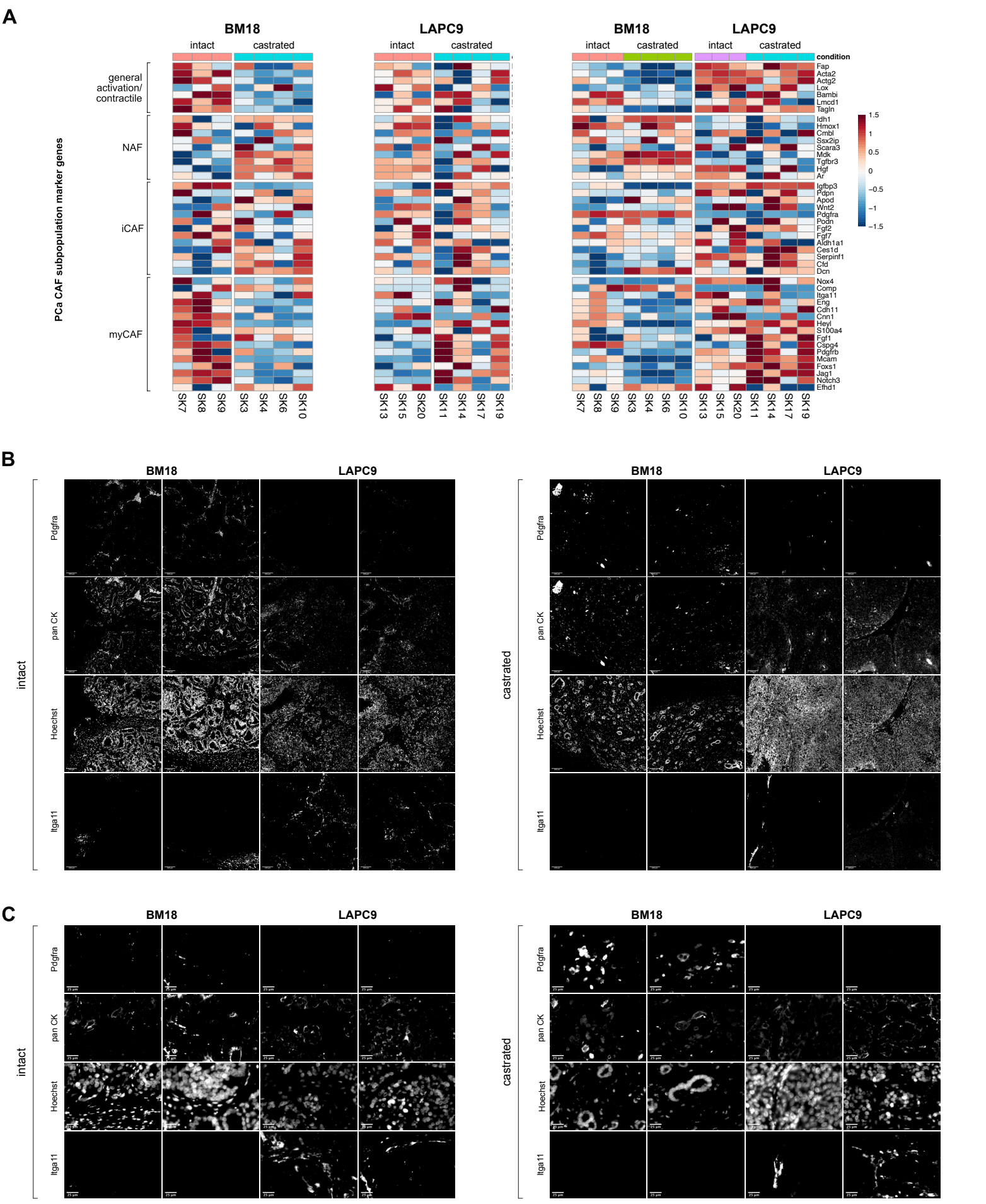

Supplemental Fig. 9